Coulomb Blockade Plasmonic Switch

Dao Xiang, Jian Wu, Reuven Gordon*

Department Electrical and Computer Engineering, University of Victoria, Victoria, BC V8P 5C2, Canada

ABSTRACT: Tunnel resistance can be modulated with bias via the Coulomb blockade effect, which gives a highly nonlinear response current. Here we investigate the optical response of metal-insulator-nanoparticle-insulator-metal structure and show switching of plasmonic gap from insulator to conductor via conquering Coulomb blockade. By introducing a sufficiently large charging energy in tunnelling gap, the Coulomb blockade allows for a conductor (tunneling) to insulator (capacitor) transition. The tunnelling electrons can be delocalized over the nano-capacitor again when a high energy penalty is added with bias. We demonstrate that this has a huge impact on the plasmonic resonance of 0.51 nm tunneling gap with ~70% change in normalized optical loss. Since this structure has a tiny capacitance, there is potential to harness the effect for high-speed switching.

KEYWORDS: Coulomb blockade, Nanoparticles, Quantum tunnelling, Switching

There has been a long history of studying the Coulomb blockade mediated quantum tunnelling, providing the fundamental insights into solutions for the conventional silicon devices and the future nanoelectronic circuits[1-9]. Conventionally, the test platforms of scanning tunneling microscopy and spectroscopy or CMOS-compatible device structures for Coulomb blockade have made past investigations limited to only low-frequency electronic characteristics.

The field of quantum plasmonics has also seen great activity in recent years due to the ability to probe the quantum properties of optical waves and their interaction with bound

oscillations of electrons at nanoscale[10-14]. It provides the accurate platform to study the ultimate limits of many applications related to plasmonics, such as harmonic generation[15-17] and optical switching[18,19]. Therefore, it is of fundamental interest to probe the discrete electron transport characteristics by an experimental method in plasmonics which is sensitive to the local carrier density. Here we use a different approach to observe the Coulomb blockade effect and show the transition of plasmonic gap from an insulating to conducting with bias.

Figure 1a shows the schematics of the nano-device consisting of 60 nm gold nanospheres trapped in a nano-gap between two electrodes. After the slit with the size of ~65 nm was fabricated in the gold slide by using focused ion beam (Hitachi FB-2100 FIB), self-assembled monolayers (SAMs) of amine-terminated alkanethiols of varying lengths were prepared on the surface of gold films, using cysteamine (30070, Sigma-Aldrich), 3-amino-1-propanethiol hydrochloride (739294, Sigma-Aldrich), 6-amino-1-hexanethiol hydrochloride (733679, Sigma-Aldrich) (referred to as “c2”, “c3”, “c6”). 3 mM solutions of the alkanethiols were prepared in anhydrous ethanol in cleaned glass containers and the gold film was immersed into the container for 18 hours, followed by rinsing with anhydrous ethanol for 15 seconds. The aqueous suspension of 60 nm diameter gold nanoparticles (EM.GC60, BBI Solutions) centrifuged at 1000 rpm to increase the concentration to 3×10^{-5} volume fraction. Nanoparticles were then immobilized electrostatically on top of the SAMs by incubating with 100 µl of the colloidal stock for 30 min followed by rinsing with deionized water for 15 seconds and drying with a slow steam of pure nitrogen gas. When drying, surface tension pulls the particles to one edge[20].

The gold sphere can be modelled as an inductor with an effective inductance L_{sph}[21]. The asymmetric junctions can be modelled as a capacitor C_1 and a tunnel junction with a tunnel resistance R_t and a capacitance C_2[22]. The tunnel resistance is modulated with bias resulting in the

response of Figure 4d. Figure 1b shows the energy band diagram for this structure at certain bias conditions where an electron tunnels to the nanoparticle. When the applied electric energy is slightly larger than the Coulomb charging energy $E_C = e^2/2C_2$, an electron will start to tunnel onto the particle. Figure 1c shows the scanning electron microscopy (SEM) image of the device and confirms the asymmetric structure.

Figure 2 shows the measurements of the normalized loss spectra when varying the voltage for different gap width a_2. Samples were mounted on a printed board circuit (PCB) and biased by the power source. A collimated white light source (LS-1-LL, Ocean Optics Inc.) was focused onto the sample by a 20× microscope objective to excite the gap modes. The transmitted light was collected at the spectrometer (QE65000, Ocean Optics Inc.) The nanoparticle normalized loss is given by

$$NL = 1 - t_{NP} / t_{slit} \tag{1}$$

where t_{NP} and t_{slit} are the transmission spectra for nanoparticles trapped in nano-slit and the slit without particles, respectively.

The self-assembled monolayers with different lengths were used as the spacer layer between the nanoparticle and the electrode to adjust the width a_2, which was confirmed with linear scattering measurements in a past work[17]. Two distinct plasmonic resonances correspond to the wide gap at short wavelength and the narrow gap at long wavelength. The most striking feature of Figure 2 is the large spectral change in (b) when the SAM layer is reduced to two carbons (c2) compared with the SAM layer with three carbons (c3) and six carbons (c6). From Figure 2e the relative change of normalized loss at resonance can be found as:

$$\frac{\left(NL(\lambda_{r,V}) - NL_{BG,V}\right) - \left(NL(\lambda_{r,0}) - NL_{BG,0}\right)}{NL(\lambda_{r,0}) - NL_{BG,0}} \tag{2}$$

where $NL(\lambda_r)$ and NL_{BG} are the normalized loss at resonance and the background of normalized loss at a longer wavelength, respectively, and so $NL(\lambda_r)$ - NL_{BG} is the peak height of normalized loss; the subscripts of V and 0 indicate the measurement with applied voltage and the measurement without applied voltage. At the resonance, the peak heights of normalized loss are 0.042 at 0V and 0.071 at 5V, respectively, and so the modulation achieved is 70%. The spectra change in c2 experiences the threshold behavior in nonlinear way, and has the lower threshold and the stronger response than c3 and c6. We attribute this to the onset of quantum tunneling and Coulomb blockade because the plasmonic resonance is very sensitive to the local carrier density in the gap.

To test if it is consistent with insulator-metal transition in tunnel junction, we completed numerical simulations. Recent works have proposed a quantum corrected model (QCM) to capture the effects of quantum tunneling in narrow gap nanostructures[23-25]. In QCM model, the gap material is changed from the dielectric to the metal of Drude model with the revised plasma frequency of $T(E_F)^{1/2}\omega_p$, where $T(E_F)$ is the transmission probability at Fermi level and ω_p is the plasma frequency of gold. Quantum corrected model (QCM) has been used to theoretically predict the saturation of plasmonic fields due to the quantum tunneling, showing good agreement with more comprehensive quantum simulations. We use the Wentzel-Kramers-Brillouin (WKB) approximation[22] of the wavefunction in the region of slowly varying potential energy to calculate the transmission probability for tunneling with the gap size a:

$$T(E) \approx \exp\left(-2\int_0^a \beta(x)dx\right)\begin{cases} = \exp\left(\frac{4}{3}\alpha\frac{\sqrt{2ma}}{e\hbar V}\left[\left(e\phi - eV + E_F - E\right)^{\frac{3}{2}} - \left(e\phi + E_F - E\right)^{\frac{3}{2}}\right]\right), & eV < \phi \\ \approx \exp\left(-\frac{4}{3}\alpha\frac{\sqrt{2ma}}{e\hbar V}\left(e\phi + E_F - E\right)^{\frac{3}{2}}\right), & eV > \phi \end{cases} \quad (3)$$

with $\beta(x) = \alpha\sqrt{\frac{2m}{\hbar^2}\left(e\phi - eV\frac{x}{a} + E_F - E\right)}$

where α = 0.65 is the factor for electron effective mass, ϕ = 1.42 eV is the barrier height (these parameters were picked from Ref. 26), E_F is Fermi energy, m is the electron mass, V is the added voltage and $\hbar$ is the reduced Planck constant. The effective Drude model can thus be used to describe the tunneling region within the gap:

$$\varepsilon = \varepsilon_\infty - \frac{\omega_g^2}{\omega\left(\omega + i\gamma_g\right)} \tag{4}$$

with $\omega_g = \sqrt{T(E_F)}\omega_p$

where ε_∞ = 2.25 is the relative permittivity of SAMs, which characterizes the residual polarization due to the background; $\omega_p = 1.37\times10^{16}$ rad/s is the plasma frequency of gold; $T(E_F)$ if the transmission probability at Fermi level; $\gamma_g = 4.07\times10^{13}$ rad/s is equal to the scattering rate of gold because though the carrier density will be changed in the gap, the scattering rate will be similar to that of the metal. The electron wavefunction is evanescent in the gap so the electron wavefunction is mainly within the metal. Therefore, the dominant scattering of the electrons comes from the scattering within the metal region and so the scattering rate does not change to first approximation. This has some relation to the superconducting state in the barrier between Josephson and Bardeen (see "note added at proof" of Ref. 27), where the Cooper pairing was not broken by scattering in the barrier region. A Drude model material was used to model the tunneling region in the gap. To estimate the accuracy, it is useful to quantify the level of convergence[28]:

$$\delta t(i) = \sqrt{\frac{\int \left(t_{NP,i} - t_{NP,0}\right)^2 d\lambda}{\int t_{NP,i}^2 d\lambda}} \tag{5}$$

where $t_{NP,0}$ is the simulated transmission spectrum for the gold nanoparticle trapped in nano-slit with mesh size of 0.051 nm and $t_{NP,i}$ represents other mesh sizes. Figure 3 shows plots of the

near-field and the level of convergence for c2. We confirm from this that the simulation has converged at 0.1 nm mesh size.

Figure 4 shows the results of full numerical calculations of normalized loss with bias added on the narrow gap using the QCM. The nonlinear change in normalized loss confirms the Coulomb blockade effect, which agrees well with our observations.

Coulomb blockade is only observed when the system satisfies two necessary conditions[22]: (1) the charging energy should exceed the thermal energy to surpass thermally excited electron tunneling, $E_C > k_BT/2$ (~12.5 meV at room temperature); (2) the tunnel resistance R_t of the junctions must be larger than the quantum resistance to suppress the quantum fluctuations, $R_t > \hbar/e^2$ (~4.1 kΩ). We only need to examine if all conditions are satisfied in the smallest gap case of c2 because it has larger capacitance and smaller resistance than c3 and c6. The capacitance is given by[29]

$$C_1 \approx C_2 = C = 4\pi\varepsilon R\sum_{n=0}^{\infty}\frac{2\sqrt{\xi(2+\xi)}}{e^{(1+2n)\mathrm{acosh}(1+\xi)}-1} \approx 3\times10^{-18}(F) \qquad (6)$$

where the ratio $\xi = a/R$ is a parameter that describes the spacing relative to the size of the conductive sphere. Thus, the tunnel capacitance satisfies the condition (1). The distance-dependent dc conductivity at the junction can be expressed by[25]

$$\sigma_0 = \frac{a}{2\pi^2}\frac{m'}{e\hbar^3}\int_0^{E_F} T(E)dE \qquad (7)$$

where m' is the effective electron mass, e is the electron charge, $\hbar$ is the reduced plank constant, and T is the transmission probability. The tunnel resistance can be estimated as $R_t = a/(\pi r_s^2\sigma_0)$≈3.8 MΩ ($r_s$ is the Wigner–Seitz radius of gold). Therefore, our system satisfies the conditions of Coulomb blockade. Here we believe we are in the few electrons regime based on the turn-on at several voltage. The number of transported electrons until 5 V is $N = C_2\Delta V/e$ ≈30

($\Delta V \approx 1.5$ V if it assumes the threshold is 2 V in c2 and half of bias voltage was added onto the tunnel capacitance).

In summary, we have observed the "turning on" of electron transport in the plasmonic structure due to the Coulomb blockade and its impact on the plasmonic resonance. The relative change of normalized loss at the resonances reaches ~70% after "turning on", indicting a large change of carrier density in the sub-nanometer gap. It is interesting to consider the time constant based on the tunnel capacitance and free-space resistance of coupled antenna $\tau = R_0 C_2 \approx 1$ (fs). This shows the potential of this effect for applications such as ultrafast optical switch[18]. It is possible that these experiments can be extended, with significant effort, to consider single particle spectroscopy, gated transport and symmetric gap geometries (with precise control of the gap). In this case, a deeper understanding of the related quantum plasmonics is expected.

AUTHOR INFORMATION

Corresponding Author

* Email: rgordon@uvic.ca.

Notes

The authors declare no competing financial interest.

Funding

This work is supported by the NSERC CREATE grant Materials for Enhanced Energy Technologies.

ACKNOWLEDGMENT

The authors acknowledge funding from the Materials for Enhanced Energy Technologies NSERC CREATE program and the NSERC Discovery Grant program.

REFERENCES

(1) Dorogi, M.; Gomez, J.; Osifchin, R.; Andres, R. P.; Reifenberger, R. *Phys. Rev. B* **1995**, *52*, 9071-9077.

(2) Andres, R. P.; Bein, T.; Dorogi, M.; Feng, S. *Science* **1996**, *272*, 1323-1325.

(3) Gittins, D. I.; Bethell, D.; Schiffrin, D. J.; Nichols, R. J. *Nature* **2000**, *408*, 67-69.

(4) Postma, H. W. C.; Teepen, T.; Yao, Z.; Grifoni, M.; Dekker, C. *Science* **2001**, *293*, 76-79.

(5) Cui, J. B.; Burghard, M.; Kern, K. *Nano Lett.* **2002**, *2*, 117-120.

(6) Park, J.; Pasupathy, A. N.; Goldsmith, J. L.; Chang, C.; Yaish, Y.; Petta, J. R.; Rinkoski, M.; Sethna, J. P.; Abruna, H. D.; McEuen, P. L.; Ralph, D. C. *Nature* **2002**, *417*, 722-725.

(7) Ray, V.; Subramanian, R.; Bhadrachalam, P.; Ma, L. C.; Kim, C. U.; Koh, S. J. *Nature Nanotech.* **2008**, *3*, 603-608.

(8) Shin, S. J.; Lee, J. J.; Kang, H. J.; Choi, J. B.; Yang, S. R. E.; Takahashi, Y.; Hasko, D. G. *Nano Lett.* **2011**, *11*, 1591-1597.

(9) Lee, S.; Lee, Y.; Song, E. B.; Hiramoto, T. *Nano Lett.* **2013**, *14*, 71-77.

(10) Brongersma, M. L.; Shalaev, V. M. *Science* **2010**, *328*, 440-441.

(11) Cuche, A.; Mollet, O.; Drezet, A.; Huant, S. *Nano Lett.* **2010**, *10*, 4566-4570.

(12) Marinica, D. C.; Kazansky, A. K.; Nordlander, P.; Aizpurua, J.; Borisov, A. G. *Nano Lett* **2012**, *12*, 1333-1339.

(13) Tame, M. S.; McEnery, K. R.; Özdemir, Ş. K.; Lee, J.; Maier, S. A.; Kim, M. S. *Nature Phys.* **2013**, *9*, 329-340.

(14) Duan, H.; Fernández-Domínguez, A. I.; Bosman, M.; Maier, S. A.; Yang, J. K. *Nano Lett.* **2012**, *12*, 1683-1689.

(15) Thyagarajan, K.; Butet, J.; Martin, O. J. *Nano Lett.* **2013**, *13*, 1847-1851.

(16) Butet, J.; Thyagarajan, K.; Martin, O. J. *Nano Lett.* **2013**, *13*, 1787-1792.

(17) Hajisalem, G.; Nezami, M. S.; Gordon, R. *Nano Lett.* **2014**, *14*, 6651-6654.

(18) MacDonald, K. F.; Sámson, Z. L.; Stockman, M. I.; Zheludev, N. I. *Nature Photon.* **2009**, *3*, 55-58.

(19) Cao, L.; Brongersma, M. L. *Nature Photonics* **2009**, *3*, 12.

(20) Kinge, S.; Crego-Calama, M.; Reinhoudt, D. N. *Chem. Phys. Chem.* **2008**, *9*, 20-42.

(21) Engheta, N.; Salandrino, A.; Alù, A. *Phys. Rev. Lett.* **2005**, *95*, 095504.

(22) Hanson, G. W. *Fundamentals of nanoelectronics*; Pearson/Prentice Hall: Upper Saddle River, 2008.

(23) Esteban, R.; Zugarramurdi, A.; Zhang, P.; Nordlander, P.; García-Vidal, F. J.; Borisov, A. G.; Aizpurua, J. *Faraday Discussions* **2015**, *178*, 151-183.

(24) Esteban, R.; Borisov, A. G.; Nordlander, P.; Aizpurua, J. *Nature Commun.* **2012**, *3*, 825.

(25) Pitarke, J. M.; Flores, F.; Echenique, P. M. *Surface Sci.* **1990**, *234***,** 1-16.

(26) Wang, W.; Lee, T.; Reed, M. A. *Phys. Rev. B* **2003**, *68*, 035416.

(27) Bardeen, J. *Phys. Rev. Lett.* **1962**, *9*, 147-149.

(28) Lu, J.; Zhou, H. *Chinese Physics B* **2016**, *25*, 090203.

(29) Crowley, J. M. *Proc. ESA Annual Meeting on Electrostatics*, 2008.

Figures

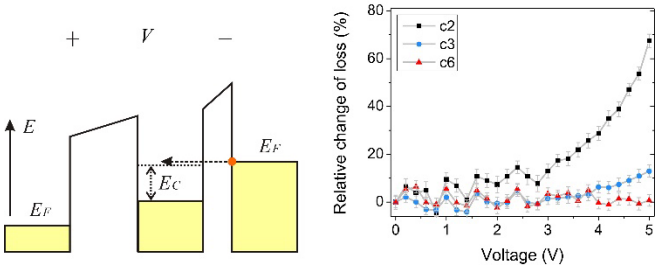

TOC figure

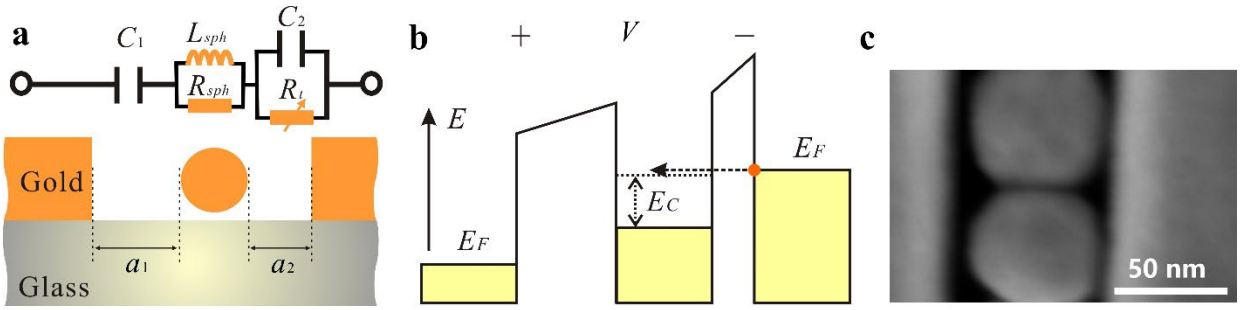

Figure 1. (a) The schematics of the double-junction structure; (b) Energy band diagram for the nano-device (the energy gap E_C exists due to the charging energy); (c) The SEM image of asymmetric structure.

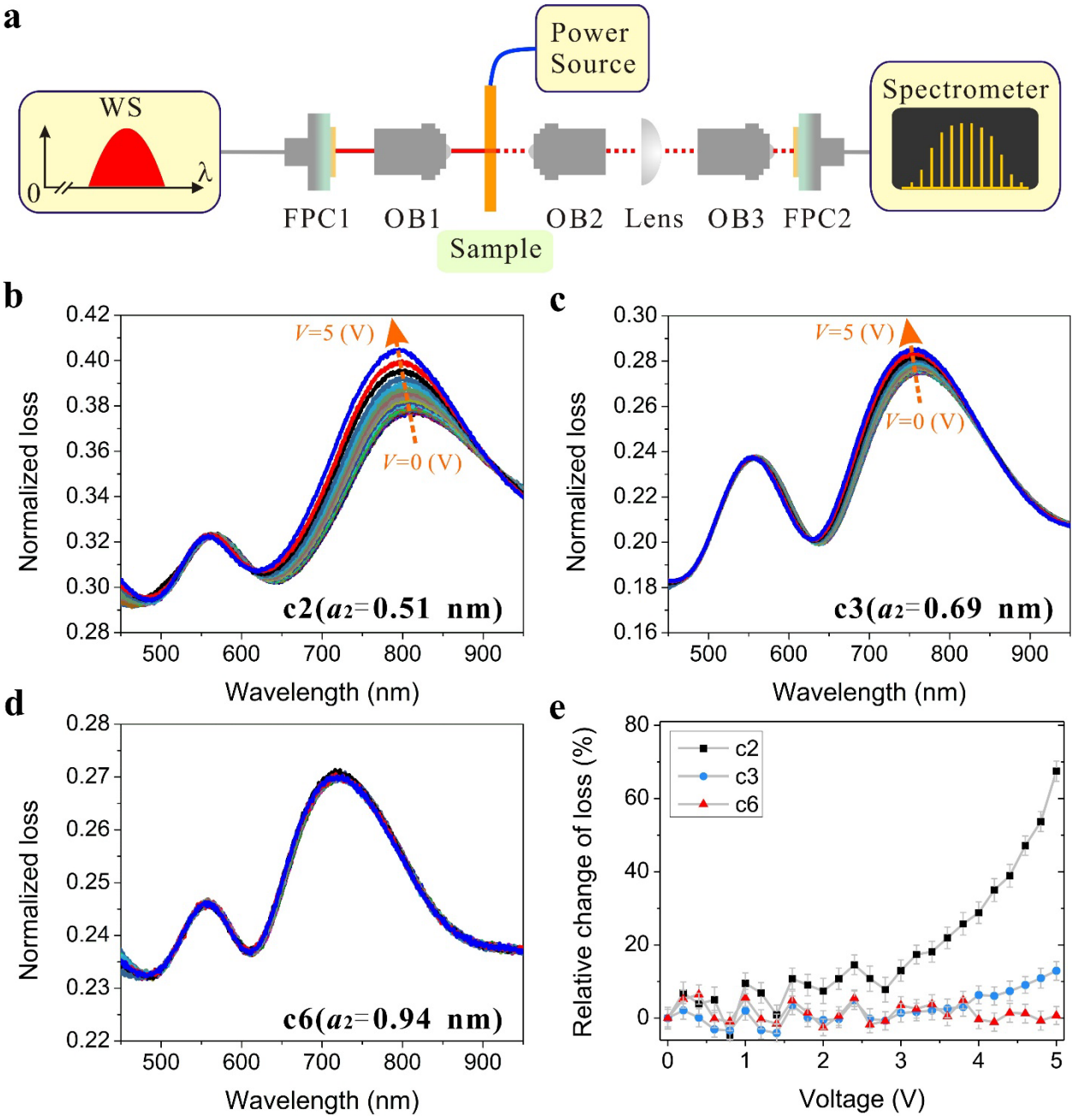

Figure 2. (a) The schematic of transmission measurement; (b, c, d) the normalized loss spectra averaged by 10 repeated measurements for nanoparticles in a slit separated by SAMs: (b) cysteamine (c2), (c) 3-amino-1-propanethiol hydrochloride (c3), (d) 6-amino-1-hexanethiol hydrochloride (c6); (e) the relative change of normalized loss at plasmonic resonance.

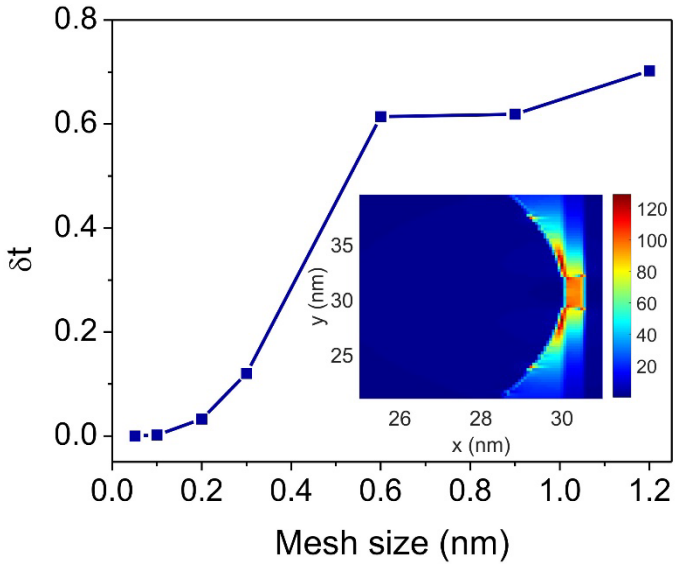

Figure 3. The level of convergence of the numerical calculation for c2 with mesh size. Inset is near-field.

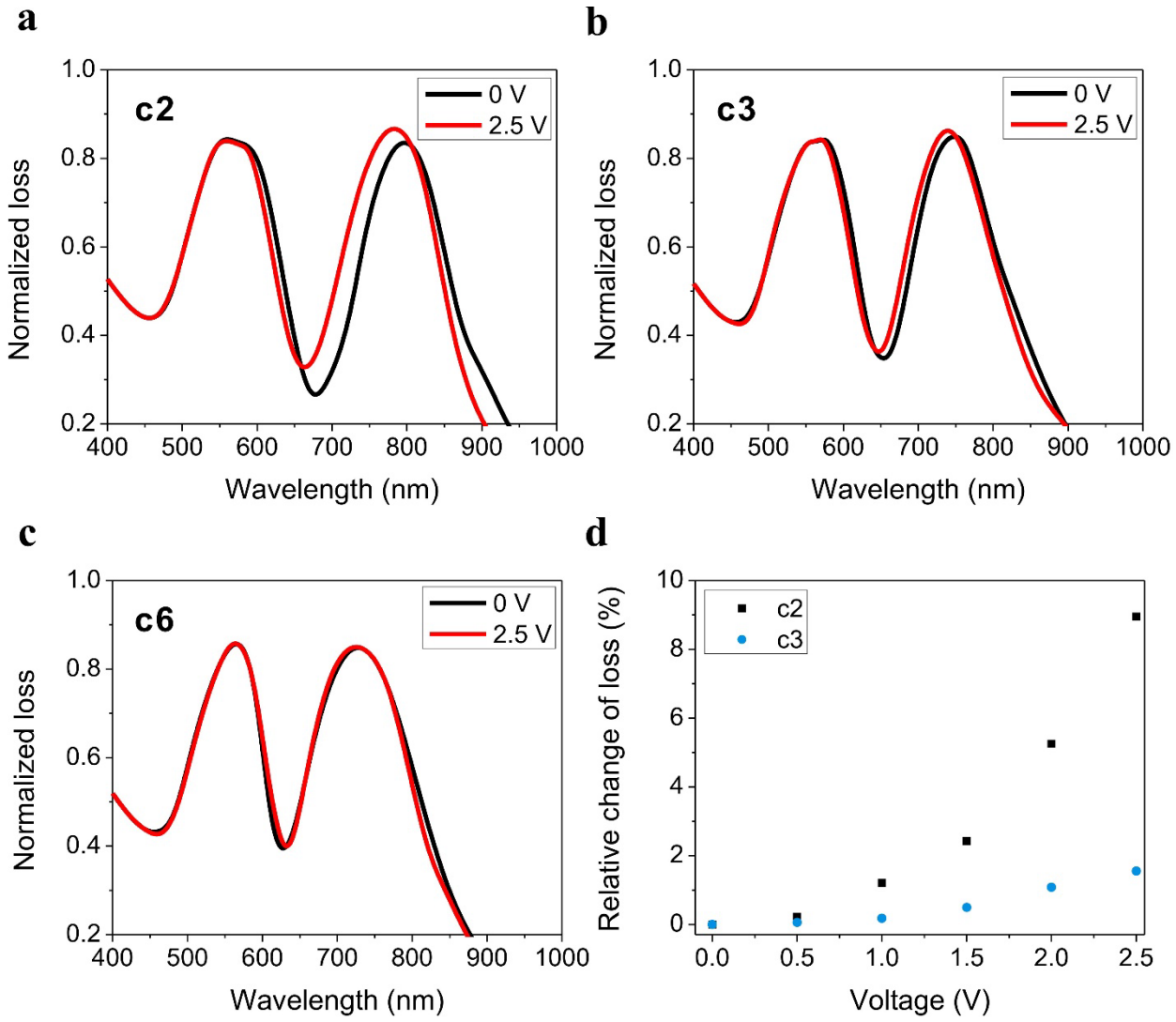

Figure 4. Simulated normalized loss for different narrow gap widths: (a) 0.51 nm (c2), (b) 0.69 nm (c3), (c) 0.94 nm (c6); (d) comparison of the relative change of normalized loss at plasmonic resonance between c2 and c3.